Unravelling Heterodyne Force Microscopy

Verbiest, G.J.

CHAPTER 4

Subsurface-AFM: Sensitivity to the Heterodyne Signal

Applying a HFM, it has been impressively de-monstrated that it is possible to obtain subsurface information: ~ 17.5 *nm large gold nanoparticles that were buried 500 nm deep, have been imaged. It is the heterodyne signal that contains the subsurface information. We elucidate, both theoretically and experimentally, the sensitivity to the heterodyne signal as a function of the tip-sample distance. This is of crucial information for experiments as the distance and, therefore, the sensitivity is tunable. We show that the amplitude of the heterodyne signal has a local maximum in the attractive part of the tip-sample interaction before it, surprisingly, reaches an even higher plateau, when the tip-sample interaction is repulsive. This can only be explained by a non-decreasing amplitude of the ultrasonic motion of the tip, although it is in full contact with the surface. We confirm this counterintuitive tip behavior experimentally even on a hard surface like Silicon.*

Most of this chapter is published in [52]

4.1 Introduction

It has always been a desire in microscopy to nondestructively image below a surface. Recent developments in scanning probe microscopy have shown the possibility to image subsurface nanoparticles on a nanometer scale [3–8, 53]. These measurements have been extended also to biological samples and cells [6, 9–12]. The technique used is called Heterodyne Force Microscopy [2, 3, 13]. A HFM uses the ultrasonic excitation of both the sample and the cantilever at slightly different frequencies, which are in the order of a few MHz. The nonlinear tip-sample interaction mixes these two ultrasonic excitations and generates a heterodyne signal at their frequency difference, called the difference frequency [3, 6–14, 31–33, 48]. Mostly the difference frequency is chosen to lie well below the fundamental resonance of the cantilever, such that the cantilever really starts to oscillate at the difference frequency. It is exactly this oscillation of the cantilever at the heterodyne difference frequency, which contains the subsurface information.

In this chapter we elucidate, both theoretically and experimentally, the sensitivity to the heterodyne signal as a function of the tip-sample distance. This is of crucial information for experiments as the distance and, therefore, the sensitivity is tunable. Moreover it paves the way for making HFM measurements quantitative.

To develop a microscope that enables the quantitative imaging of subsurface structures at the nanoscale, detailed knowledge is crucial on the cantilever dynamics in close vicinity to a vibrating surface as well as on the propagation of the ultrasonic waves through the sample. The effect of a vibrating surface on a *static* cantilever has been investigated [43–47], but the case were the cantilever is also oscillating at an ultrasonic frequency still lacks understanding, although an analytical approach was explored [32]. It has been shown that the ultrasonic wave propagating through the sample is Rayleigh scattered by subsurface nanoparticles (see Chap. 2 or [28]). The amplitude contrast generated by a nanometer sized subsurface scatterer is negligible, but the generated phase contrast should be detectable, as it is in the order of a few millidegrees (see Chap. 2 or [28]). It is to mention here that a sufficiently strong signal amplitude is required for a proper phase detection. Still the main question remains how the cantilever is able to pick up both the amplitude and the phase of the ultrasonic wave after it has propagated through the sample.

Recent work by Tetard et al. (TET) [33] describes a generalization of Heterodyne Force Microscopy, called Mode Synthesizing Atomic Force Microscopy (MSAFM), in which both the cantilever and sample are excited at frequencies, ω_t and ω_s respectively, far above the fundamental resonance of the cantilever. Using a numerical method TET show how the nonlinear tip-sample interaction generates a signal at the difference frequency $\omega_{\text{diff}} = |\omega_s - \omega_t|$ in the atractive

part of the tip-sample interaction and compare this with their experimental results. They conclude that the generation of the amplitude of ω_{diff} *appears to more crucially depend on the particular power law of the long-range forces* than on the short-range repulsive forces.

Here we show, by contrast, how the *repulsive* interaction does generate a signal at the difference frequency ω_{diff}, with an amplitude that is even stronger than the peak observed in the attractive Van-der-Waals regime. TET choose a volume integrated Lennard-Jones potential (LJ-model), which is also called the Bradley model of rigid contact, see Sect. 1.4. This model has a divergence at zero tip-sample distance. To prevent divergences in their simulation they constrained the tip-sample distance such that the cantilever cannot come closer to the sample than a certain distance d_0. This restriction is indeed necessary, but by choosing the numerical parameters more carefully, it is possible to study the cantilever dynamics even deep in the repulsive part of the tip-sample interaction. In our simulations we calculate not only the LJ-model, which shows a significant amplitude of the difference frequency in the repulsive regime, but we also calculate with the Derjaguin-Muller-Toporov interaction (DMT-model), see Sect. 1.4 and [23], where indentation of the sample is allowed to a certain extent and there is no divergence at zero tip-sample separation. Usually the DMT-model is a more realistic description of the tip-sample interaction, especially for recent experiments, using MSAFM, performed on soft biological samples [12, 14, 33]. To confirm our simulations, we performed measurements and find an excellent agreement between our numerical calculations and our experiments. Finally we show, experimentally for the first time, that the ultrasonic amplitude of the cantilever/tip remains almost constant, even if the cantilever is pushed such that the tip is deep in the repulsive regime. This result clarifies the observed amplitude behavior of the difference frequency and might explain the particular choice of many HFM experiments [3, 6–14, 31–33, 48], in which the cantilever is brought in full contact with the sample.

4.2 Numerical Calculation of the Heterodyne Signal

Figure 4.1 shows a schematic view of the setup used in both the experiments and the numerical simulations. The cantilever is excited at an angular frequency ω_t with amplitude A_t and phase ϕ_t, while the sample is excited at an angular frequency ω_s with amplitude A_s and phase ϕ_s. In an experiment, the cantilever's base is continuously moved towards the sample and out again. During this movement, the nonlinearity in the tip-sample interaction generates a drive force on the cantilever at the difference frequency $\omega_{\text{diff}} = |\omega_s - \omega_t|$, of which we detect both the amplitude A_{diff} and the phase ϕ_{diff} in the cantile-

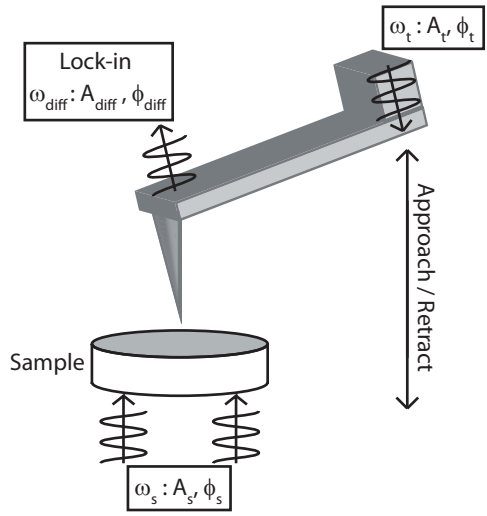

Figure 4.1: Scheme of the HFM setup of our experiments and our numerical simulations. The sample is excited at a frequency (ω_s) with a fixed amplitude (A_s) and phase (ϕ_s), and the cantilever is excited at a frequency (ω_t) with amplitude (A_t) and phase (ϕ_t). The amplitude (A_{diff}) and the phase (ϕ_{diff}) of the signal at the difference frequency (ω_{diff}) is detected via a lock-in method. During an experiment, in which we approach and retract the cantilever from the surface, only the z-position of its base is moved.

ver's motion (response to the drive force) via a lock-in method in both the simulations and the experiments.

To receive a proper description for the tip-sample distance z, one has to realize that we vary the cantilever's base z_b in both the simulations and the experiment. Next, to account for a possible bending of the cantilever, we include the deflection δ (which is a function of the spring constant of the cantilever), in addition to the ultrasonic motion of both the cantilever and the sample. Finally, we take into account the response of the cantilever to the drive force at the difference frequency ω_{diff} and get

$$\begin{aligned} z =& z_b + \delta + A_{\text{diff}} \cos(\omega_{\text{diff}} t + \phi_{\text{diff}}) \\ &+ A_s \cos(\omega_s t + \phi_s) + A_t \cos(\omega_t t + \phi_t). \end{aligned} \tag{4.1}$$

To enable a proper comparison between the simulations and the experiments, we subtract an offset in z_b such that $z_b = 0$, if the deflection $\delta = 0$ during the approach cycle of the cantilever to the surface. This is exactly the point, at which the *effective* interaction on the tip changes sign from an attrac-

tive interaction to a repulsive interaction [1].

Let us first discuss our numerical simulations, in which we used a mode expansion to model the cantilever dynamics. In the mode expansion the motion of the cantilever is expressed as the sum over its eigenmodes [50, 51], in which each eigenmode is characterized by a resonance frequency, a corresponding quality factor Q, and a mode shape. A full description of our approach can be found in Chap. 3 and in [42]. In our calculations we assumed a Silicon cantilever with a stiffness of 2 N/m and a tip radius of $R = 5$ nm. The fundamental mode has a resonance frequency of 73.4 kHz and a quality factor Q of 150. In our numerical simulations, the cantilever is ultrasonically excited at $\omega_t/2\pi = 3.1705$ MHz with an amplitude $A_t = 10$ nm, while the sample is ultrasonically excited at $\omega_s/2\pi = 3.1695$ MHz with an amplitude $A_s = 0.1$ nm. Both ultrasonic excitations are far away from any resonance and lie between the resonance frequencies of the 4^{th} and 5^{th} eigenmode of the cantilever. The difference frequency ω_{diff} is 1 kHz, which is well below the fundamental mode of the cantilever.

As mentioned above, we used two different types of tip-sample interactions in our numerical simulations: the DMT-model as described by Eq. 4.2, and the LJ-model as decribed by Eq. 4.3. The LJ-model was also used by TET. In both models, the tip-sample interaction is characterized by the Hamaker constant H and the distance a_0, at which the repulsive part of the tip-sample interaction becomes significant. The DMT-model has one additional parameter, which is the effective tip-sample elasticity described by an effective Young's modulus E_{eff}. In our numerical simulations, we assumed $H = 8.2 \cdot 10^{-20}$ J, $a_0 = 0.45$ nm, and $E_{eff} = 100$ GPa. The value for E_{eff} corresponds to a Silicon tip indenting a Silicon sample.

$$F_{ts}^{DMT}(z) = \begin{cases} -\frac{HR}{6a_0^2} + \frac{4}{3}E_f\sqrt{R}(a_0 - z)^{3/2} & \text{if } z < a_0 \\ -\frac{HR}{6z^2} & \text{if } z \geq a_0 \end{cases} \tag{4.2}$$

$$F_{ts}^{LJ}(z) = \frac{2HR}{9a_0^2}\left(\frac{1}{4}\left[\frac{a_0}{z}\right]^8 - \left[\frac{a_0}{z}\right]^2\right) \tag{4.3}$$

Next to the LJ- and DMT-model, one could also consider the so-called the Maugis-Dugdale (M-D-) model or the Johnson-Kendall-Roberts (JKR-) model. The difference between the DMT-, the M-D-, and the JKR-model is mainly the treatment of the attractive part of the tip-sample interaction. An overview of the different models can be found in Sect. 1.4 and [54, 55]. The applicability of a certain model is fully determined by an elasticity parameter λ and a normalized load P [27]. These parameters depend on the radius R of the tip, an effective elasticity, the effective work of adhesion, the "Dugdale" stress,

[1] The offset is given by $A_s + A_t + A_{\text{diff}}$. To avoid an unnecessary complication (nonlinear rescaling) of the x-axes in the plots of this chapter, we neglect for these axes the variations in both A_t and A_{diff}.

and the applied load. For very large loads, it is sufficient to use the Hertzian contact model. As the DMT-, M-D-, and JKR-model all include a Hertzian contact repulsion, these models are applicable for a larger range of forces not only describing the high load regime correctly but also the low load part with attractive interaction. The LJ-model is different in this sense, as it contains a pure Lennard-Jones potential and not a Hertzian contact description. Based on the values for Silicon (material of our tip and sample) and on a tip radius of 5 nm, which characterizes the tip-sample interaction in our simulations and describes also our experiments, we find that $\lambda = 0.01$. If we take into account also the variations in tip radii (see below), we receive values for λ between 0.007 and 0.014 and conclude that $\lambda = 0.01$ properly describes all cases discussed in the current chapter. Considering the other parameter, the normalized load P, we realize that we have to deal with a large range between -2 and 200, as we study the amplitude A_{diff} as a function of the contact force. The determination of the appropriate model can be nicely read off from Fig. 1.8. For $\lambda = 0.01$, the LJ-model should be used for loads smaller than 0.6 nN, while the DMT-model should be applied for higher contact loads. We safely can neglect the M-D- and the JKR-model, as they are both only applicable at significantly higher λ values: $\lambda = 0.086$ and $\lambda = 5.6$, respectively. We conclude that it is sufficient to consider only the LJ-model and the DMT-model and to address a comparison between those results.

Figure 4.2 shows the ω_{diff} amplitude A_{diff} for both the DMT-model (upper panel) and the LJ-model (lower panel) as a function of the height of the cantilever's base z_b (that determines tip-sample distance z). The vertical dashed lines indicate the distances where the cantilever touches the sample and starts to feel the repulsive part of the tip-sample interaction. For both the DMT-model and the LJ-model, we see that there is indeed, as also shown by TET, a peak in the attractive part of the tip-sample interaction. However, with decreasing cantilever height z_b, when the tip starts to feel the repulsive interaction, the amplitude A_{diff} of ω_{diff} converges to a plateau, also for the LJ-model. Both plateau's are even higher than the peak in the attractive Van-der-Waals regime. This indicates the importance of the repulsive part of the tip-sample interaction. We conclude that there is almost no difference in A_{diff}, if determined by either the DMT- or the LJ-model.

To address the influence of the shape of the cantilever's tip, we evaluated the amplitude A_{diff} considering the DMT-model for three different tip radii, $R = 15$ nm (black), $R = 5$ nm (grey), and $R = 1.67$ nm (light grey) as a function of the tip-sample distance, see Fig. 4.3. We observe similar curves as shown in Fig. 4.2 and note that the height of the peak in the attractive part of the tip-sample interaction depends on the tip radius R, whereas the height of the plateau in the repulsive part converges to the same value for all R.

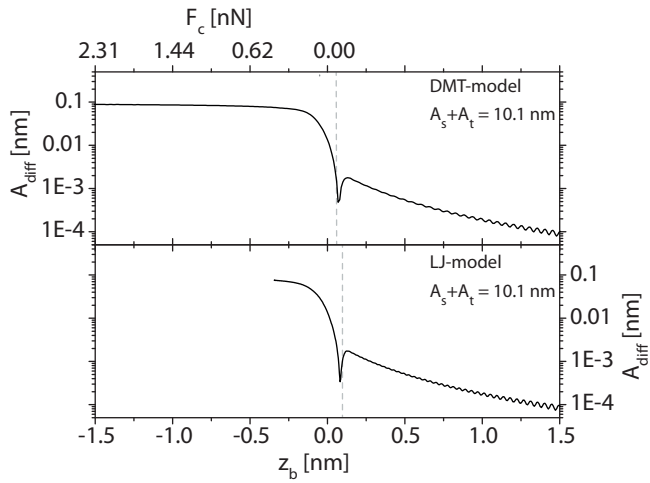

Figure 4.2: Numerical simulations ($\omega_t/2\pi = 3.1705$ MHz, $A_t = 10$ nm, $\omega_s/2\pi = 3.1695$ MHz, and $A_s = 0.1$ nm): the amplitude A_{diff} of ω_{diff} for the DMT-model (top) and the LJ-model (bottom) as a function of the height of the cantilever's base z_b (that determines tip-sample distance z). Note that the x-axis is not linear in z due to the cantilever's deflection δ. $z_b = 0$ defines the border between the attractive and the repulsive regime, at which the *effective* force on the cantilever is zero, whereas the vertical dashed lines indicate the distances, at which the cantilever touches the sample and starts to feel the repulsive part of the tip-sample interaction. When approaching the surface, both models show a peak in the attractive part of the tip-sample interaction before an even higher plateau is reached in the repulsive part.

The inset of Fig. 4.3 shows that the height of the local maximum A_{diff}^{peak} in the attractive part of the tip-sample interaction is directly proportional to R. The reason for this linearity becomes obvious, if one realizes that the adhesion in the attractive part of the tip-sample interaction scales with the tip radius R. This can also be seen in Eq. 4.2: the tip-sample interaction for $z > a_0$ is directly proportional to R. Accordingly, also A_{diff} is proportional to R.

A similar argumentation implies that the height of the plateau of the amplitude A_{diff} depends on the properties of the repulsive part of the tip-sample interaction. Therefore, one would expect that the height of the plateau is proportional to $\sqrt{R}$, see Eq. 4.2. However, it was shown in Chap. 3 (or [42]) that the height of the plateau can be calculated on the basis of A_s and A_t only, without any knowledge on R. The reason for this is that the amplitude A_{diff} is in saturation on the plateau. The chosen variation in tip radii R in this chapter does not lower A_{diff} below its saturation value implying even that the height of the plateau is independent of all other parameters characterizing the tip-sample interaction (such as the tip radius R).

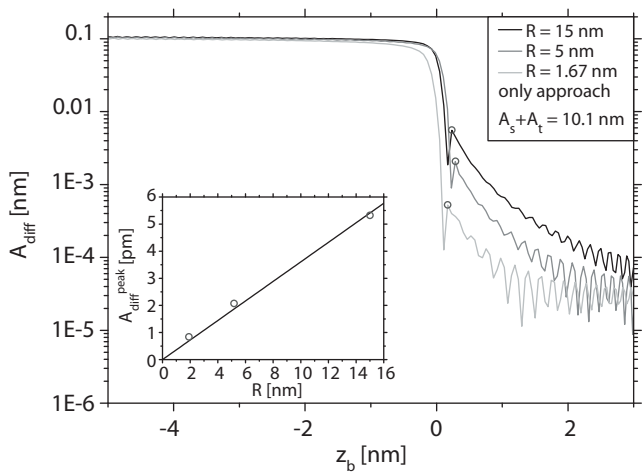

Figure 4.3: Numerical simulations: the amplitude A_{diff} of ω_{diff} for the DMT-model as a function of the height of the cantilever's base z_b (that determines tip-sample distance z). Note that the x-axis is not linear in z due to the cantilever's deflection δ. Different colors indicate different tip radii R: 15 nm (black), 5 nm (grey), and 1.67 nm (light grey). The inset shows that the height of the local maximum A_{diff}^{peak} in the attractive part of the tip-sample interaction is directly proportional to R. The height of the plateau is independent of R.

One might also consider different macroscopic tip shapes and their corresponding change in the tip-sample interaction, as described in [56, 57]. These shapes will not have an influence on the height of the plateau in the repulsive regime, as A_{diff} is in saturation. In the attractive regime, however, we do expect an influence on the local maximum A_{diff}^{peak}. Such an influence is, in first approximation, well modelled by a variation in tip radius R, which we did (see above).

4.3 Experimental Detection of the Heterodyne Signal

Let us now discuss the experiments. In analogy to our numerical simulations, we performed the experiment with a standard 2 N/m cantilever on a freshly cleaned Silicon sample. The cantilever was an OMCL-AC240TN of Olympus [58], which has a length of 240 μm, a width of 40 μm, a thickness of 2.3 μm, a typical resonance frequency of 73.4 kHz, and a tip radius of 5 nm, which we confirmed with a high resolution Scanning Electron Microscope. The sample was glued with Crystalbond 509 onto a piezo element, which has a free

resonance in the order of 4 MHz. In the same way, the cantilever was glued onto a similar piezo element that was mounted in a custom-made cantilever holder. The cantilever and the sample were excited at 2.870 MHz and 2.871 MHz respectively, which are far from any resonances of the cantilever. The experiments were performed on a Nanoscope V Multimode 8 from Bruker [16]. The motion of the cantilever is measured via the standard optical beam deflection method. The slope of the mode shape at the cantilever's free end is proportional to the sensitivity. Since we obtain the slopes of all higher eigenmodes of the cantilever from the numerical calculations, we estimate the sensitivity of the photodiode for the 5^{th} mode to be 12.6 times higher than the sensitivity for the first mode. This method is valid, because the higher eigenmodes are insensitive to the tip-sample interaction such that the mode shape does not significantly change when the tip gets into contact with the sample: considering the forces applied in all experiments that are described in this thesis, we only have a maximum frequency shift of $\sim$ 10 kHz of the 5th mode at a maximum contact force $F_c = 163$ nN (see also Fig. 5.4, which shows the frequency shifts of the different modes as a function of the applied load at the end of the cantilever in terms of the normalized tip-sample stiffness I_1/k). In this way, we obtained a sensitivity of 67.7 nm/V at 71.8 kHz and 5.4 nm/V at 2.87 MHz. This leads to a measured amplitude A_t of the cantilever at 2.87 MHz of approximately 0.96 nm. The amplitude A_s of the sample vibration was not measured. However, as the plateau in the repulsive regime depends only on the amplitudes of both the cantilever A_t and the sample A_s (see Chap. 3 and [42]), we can estimate the sample amplitude A_s to be 0.32 nm in our experiments. During the experiments we never saw the excitation ω_s of the sample in the cantilever's motion, which we attribute to the unfavorable ratio of the cantilever stiffness and the sample stiffness at MHz frequencies.

In Fig. 4.4 we see the amplitude A_{diff} of ω_{diff} in the top panel and the static cantilever deflection in the bottom panel. The amplitude A_{diff} shows qualitatively the same features as in the simulations presented in Fig. 4.2. It reaches a local maximum in the attractive regime, i.e. negative deflection, indicated with the vertical lines. In the repulsive regime, the amplitude rises to a plateau, which is in excellent agreement with our numerical simulations. Even at a deflection of 10 nm, which corresponds to a contact force of 20 nN and an indentation of 0.9 nm, the value of the plateau remains constant. However, as soon as the tip is indented approximately $A_s + A_t$, the cantilever is in contact with the sample during the complete ultrasonic oscillations. As a consequence, the tip-sample interaction approaches a more linear dependence (as it is deeper in the repulsive regime). This implies that the generation of the nonlinear heterodyne signal, A_{diff}, starts to decrease to zero, as $\partial F_{ts}/\partial z$ approaches zero causing also that I_2 in Eq. 5.27 as well as A_{diff} in Eq. 5.24 approach zero. Therefore, the plateau does not remain constant and is expected

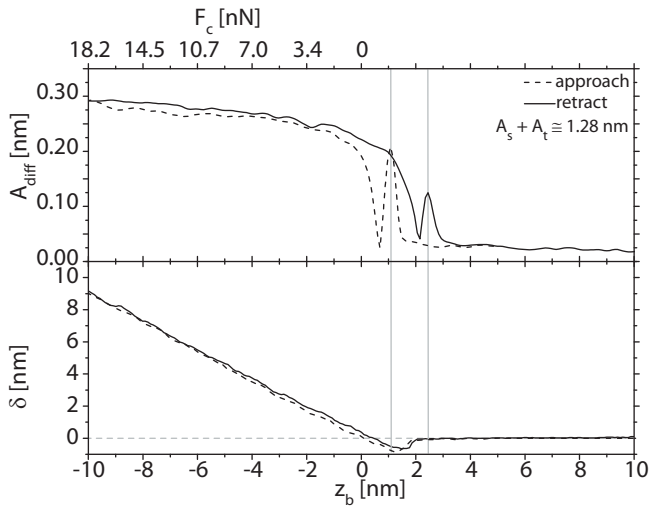

Figure 4.4: Experiment: the amplitude A_{diff} of ω_{diff} (top) and the static cantilever's deflection δ (bottom) measured on Silicon as a function of the height of the cantilever's base z_b (that determines tip-sample distance z). Note that the x-axis is not linear in z due to the cantilever's deflection δ. $z_b = 0$ defines the border between the attractive and the repulsive regime, at which the *effective* force, F_c, on the cantilever is zero. It is impossible to indicate the positions, at which the cantilever touches the surface, due to the missing information on F_{ts} in the experiment. The solid vertical lines indicate the positions of the local maxima of A_{diff} and demonstrate that these maxima are indeed located in the attractive part of the tip-sample interaction ($\delta < 0$). Please note that A_{diff} converges to a plateau in the repulsive part of the tip-sample interaction.

to decrease for large indentations.

An unexpected result of our numerical simulations is that the ultrasonic amplitude of the tip, A_t, remains almost constant while approaching and even indenting the sample; for details see Chap. 3 and [42]. The reason for this is the extremely high spring constant of the 5^{th} eigenmode of the cantilever (~ 1000 N/m) with respect to the spring constant of the bending mode of the cantilever, which is only 2 N/m in this case. As a consequence of this, the cantilever bends when getting in full contact with the sample, thereby leaving the high frequency motion unaltered. Although suggested [5, 53], a constant ultrasonic cantilever amplitude at MHz frequencies was never observed in experiments before, and might be surprising, as one intuitively would expect that tip-sample damping reduces the amplitude A_t significantly. In the bottom panel of Fig. 4.5, we actually do see that A_t remains (almost) constant while approaching and deeply indenting the tip into the sample in our experiment. In full contact, we still have

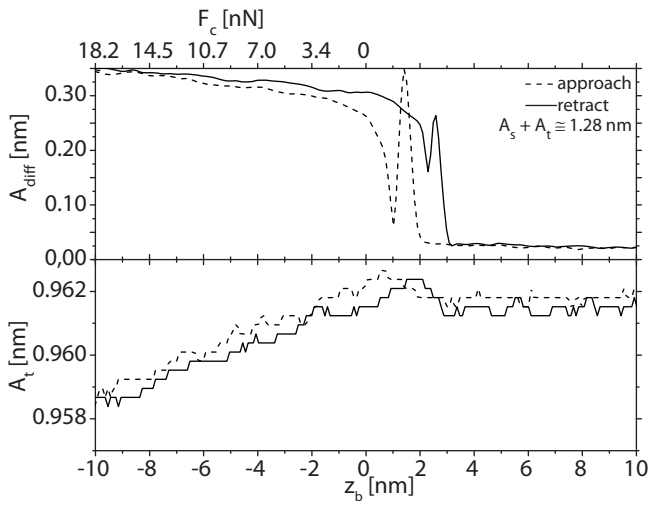

Figure 4.5: Experiment: the amplitude A_{diff} of ω_{diff} (top) and the amplitude A_t of ω_t (bottom) measured on Silicon as a function of the the height of the cantilever's base z_b (that determines tip-sample distance z). Note that the x-axis is not linear in z due to the cantilever's deflection δ. $z_b = 0$ defines the border between the attractive and the repulsive regime, at which the *effective* force, F_c, on the cantilever is zero. It is impossible to indicate the positions, at which the cantilever touches the surface, due to the missing information on F_{ts} in the experiment. Please note that A_t stays almost constant even deep in the repulsive part of the tip-sample interaction: it reduces only to 99.7% of its free amplitude.

99.7% of the free amplitude left while the static deflection is as large as ~ 10 nm. Although we see that the tip-sample interaction starts to reduce A_t when the cantilever comes into contact, this reduction is indeed very small, because of the high spring constant and the bending of the cantilever. We attribute the reduction in amplitude to a change in damping in the tip-sample interaction. As the quantification of tip-sample damping is a hot topic in nanoscale friction [59], and as the observed reduction of A_t in our measurements is larger than the noise, we estimate from Fig. 4.5 the change in the quality factor Q of the cantilever's 5^{th} eigenmode: the quality factor decreases from $Q = 92$ (based on our simulations) to $Q = 20$ when the tip is in full contact with the sample (see Appx. 4.A). Such a strong decrease is comparable to the results found by Maier et al. [59].

4.4 Conclusion

In conclusion, we have set a next step to understand the detection mechanism in a HFM. We performed both numerical simulations and experiments of the cantilever/tip motion to get insight into the difference frequency generation that contains the subsurface information.

The numerical simulations showed that the amplitude of the difference frequency reaches a local maximum in the attractive part of the tip-sample interaction, which is in agreement with TET. Contrarily to TET, we found that the amplitude of the difference frequency reaches a pleateau in the repulsive part of the tip-sample interaction in both the LJ-model and the DMT-model. This shows that the repulsive part of the tip-sample interaction is more important than previously thought and could possibly explain why most experimental MSAFM and HFM attempts are performed such that the cantilever is in full contact with the sample for some time during its oscillation.

Furthermore, we performed experiments on a Silicon surface and found an excellent agreement with our numerical simulations. The experiments showed that the amplitude of the difference frequency A_{diff} first reaches a local maximum in the attractive part of the tip-sample interaction before it reaches a plateau in the repulsive part of the tip-sample interaction. The value of the plateau does not decrease even at a contact force of 20 nN, which equals a tip-sample indentation of ~ 0.9 nm and a cantilever's base offset z_b of 10 nm. However, as we will see in Figs. 6.3, 6.12, and 6.14, the difference amplitude A_{diff} decreases to zero for indentations approximately equal to $A_s + A_t$, due to the decrease of I_2 to zero (see Eq. 5.27).

Finally, the numerical simulations showed that the amplitude of the ultrasonic cantilever excitation A_t stays (almost) constant, even if the cantilever indents deep into the sample. We are the first to show an experiment confirming this counterintuitive result: 99.7% of the free amplitude is remained while the tip is in full contact with the sample. This implies that tip-sample damping is not important for off resonance excitations schemes, even though the damping is altered significantly.

Our simulations and experiments are the first steps towards quantitative HFM measurements, which is necessary for the development of a scanning probe microscope that delivers true 3D subsurface resolution on the nanometer scale.

Appendices of Chapter 4

4.A Estimation of the Quality Factor Reduction

As the observed reduction of A_t in our measurements is larger than the noise, we estimate from Fig. 4.5 the change in the quality factor Q of the cantilever's 5^{th} eigenmode. We start with the transfer function, which transfers a given force on the cantilever into a corresponding amplitude, at the frequency ω_t of a single eigenmode of the cantilever:

$$H(\omega_t) = \frac{\Phi_n(L)^2}{\sqrt{(\omega_t^2 - \omega_n^2)^2 + \left(\frac{\omega_n \omega_t}{Q_n}\right)^2}} \tag{4.4}$$

, in which ω_n is the resonance frequency of the n^{th} eigenmode, which has a corresponding quality factor Q_n, and mode shape $\Phi_n(x)$. While the cantilever's tip indents the sample, we do not change the drive force on the cantilever at the ultrasonic tip frequency ω_t. As a consequence, we can relate a change in vibration amplitude at the frequency ω_t to either a change in resonance frequency ω_n or a change in quality factor Q_n. As we excite the cantilever off resonance with a frequency of several MHz, we can neglect a shift in resonance frequency, as argued in Chap. 3.3. We thus assume the vibration amplitude A_t at frequency ω_t to be a function of tip-sample damping only:

$$A_t(z) = \frac{\alpha}{\sqrt{1 + \beta/Q(z)^2}} \tag{4.5}$$

, in which α and β are defined as follows

$$\alpha = \Phi_n(L)^2 F_d / |\omega_t^2 - \omega_n^2| \tag{4.6}$$

$$\beta = ((\omega_n \omega_t)/(\omega_t^2 - \omega_n^2))^2 \tag{4.7}$$

We can use Eq. 4.5 to calculate the reduction of the quality factor of the n^{th} eigenmode. We know the free quality factor $Q_n = Q(z = \infty)$ and the free vibration amplitude $A_{free} = A_t(z = \infty)$, from which we can determine $Q(z)$, if $A_t(z)$ is evaluated by dividing their corresponding transfer functions given in Eq. 4.5.

$$x^2 = \left(\frac{A_t(z)}{A_t(z = \infty)}\right)^2 = \frac{1 + \beta/Q(z = \infty)^2}{1 + \beta/Q(z)^2} \tag{4.8}$$

After rearranging this formula, we obtain an expression for $Q(z)$:

$$\frac{Q(z)}{Q(z = \infty)} = \sqrt{\frac{\frac{\beta}{Q(z=\infty)^2} x^2}{\frac{\beta}{Q(z=\infty)^2} x^2 + 1 - x^2}} \tag{4.9}$$

In our experiment, we excited the cantilever between the 4^{th} and 5^{th} eigenmode. If we use the transfer function of the 5^{th} eigenmode. We have the following parameters: $x = 0.997$, $\omega_t/2\pi = 2.87$ MHz, $\omega_5/2\pi = 3.9$ MHz, and $Q_5 = 92$. By using these parameters in Eq. 4.9, we obtain the following reduction for the quality factor: $Q(z)/Q_5 = 0.22$.

We can do the same calculation for the 4^{th} eigenmode. With $x = 0.997$, $\omega_t/2\pi = 2.87$ MHz, $\omega_5/2\pi = 2.4$ MHz, and $Q_4 = 146$, we obtain a reduction of the quality factor: $Q(z)/Q_4 = 0.24$.

In reality, the off resonance motion should be described by a superposition of the 4^{th} and 5^{th} eigenmode. However, as the results are similar between the estimations for the 4^{th} and 5^{th} eigenmode, it is justified to describe the change in damping with a single mode only in this case.